DOI: 10.1002/zaac.201200555

The Periodate-Based Double Perovskites M_2NaIO_6 (M = Ca, Sr, and Ba)

Frank Kubel,*[a] Nicole Wandl,[a] Mariana Pantazi,[a] Vincenza D'Anna,[b] and Hans Hagemann[b]

Keywords: Barium; Strontium; Calcium; Sodium *ortho*-periodates; Chemical stability; Raman spectroscopy; DFT calculations

Abstract. The crystal structures of the M_2NaIO_6 series (M = Ca, Sr, Ba), prepared at 650 °C by ceramic methods, were determined from conventional laboratory X-ray powder diffraction data. Synthesis and crystal growth were made by oxidizing I^- with $O_2^{(air)}$ to I^{7+} followed by crystal growth in the presence of NaF as mineralizator, or by the reaction of the alkali-metal periodate with the alkaline-earth metal hydroxide. All three compounds are insoluble and stable in water. The barium compound crystallizes in the cubic space group *Fm3m* (no. 225) with lattice parameters of a = 8.3384(1) Å, whereas the strontium and calcium compounds crystallize in the monoclinic space group $P2_1/c$ (no. 14) with a = 5.7600(1) Å, b = 5.7759(1) Å, c = 9.9742(1) Å, β = 125.362(1)° and a = 5.5376(1) Å, b = 5.7911(1) Å, c = 9.6055(1) Å, β = 124.300(1)°, respectively. The crystal structure consists of either symmetric (for Ba) or distorted (for Sr and Ca) perovskite superstructures. Ba_2NaIO_6 contains the first perfectly octahedral $[IO_6]^{5-}$ unit reported. The compounds of the *ortho*-periodates are stable up to 800 °C. Spectroscopic measurements as well as DFT calculations show a reasonable agreement between calculated and observed IR- and Raman-active vibrations.

Introduction

Double perovskites are a fascinating structural family with many different properties. They can be used in applied science as solid oxide fuel cell material [e.g. Sr_2MMoO_6 (M = Co, Ni) as anode materials].[1] They have interesting magnetic properties as in ferromagnetic Ca_2CrSbO_6 and antiferromagnetic Sr_2CrSbO_6[2], ionic conductivity as in $(Sr_{0.5}Ca_{0.5})(Ca_{0.5}Sb_{0.5})O_{3-\delta}$[3] or luminescence at room-temperature as observed for Ba_2MgWO_6 and Ba_2ZnWO_6.[4] Disorder was studied in spin glass double perovskites Sr_2CaReO_6 and Sr_2MgReO_6.[5] Further they appear as phosphor host materials as found for Ca_2LaMO_6 (M = Sb, Nb, Ta) doped with Eu^{III} to give a red phosphor.[6]

Double perovskites are complex oxides $A_2BB'O_6$, named after the mineral perovskite $CaTiO_3$. Here the B and B' cations are ordered in a rock salt manner, resulting idealized in a *Fm3m* cubic structure with twice the length of the ABX_3 perovskite subcell. The B-site ordering is driven by size and charge difference between the B and B' cations. For double perovskites with variations of A, B and B', several subgroups of the double perovskite cell are possible and summarized in the literature.[7] High symmetry iodine compounds have been shown to be suitable sources for ^{129}Xe Mössbauer spectroscopy.[8]

Literature data reported two different syntheses methods but no structural characterization for the compound Ba_2NaIO_6.[9] In this work, we present the structures of some periodate based double perovskites and the A-size driven deviation from the idealized cell.

Results and Discussion

Crystal Structures

Starting values of the atomic positions were taken from the mineral elpasolite K_2NaAlF_6[10] and standardized Cryolite Na_3AlF_6.[11] The refinements converged to reasonable R_{Bragg} values of ca. 2 %. Observed, calculated, and difference pattern are given in Figure 1. A texture model was successful applied (TOPAS).[12] For Sr_2NaIO_6, several models with similar R_{Bragg} values, but different oxygen positions were calculated due to false minima in the refinement, as the structure is close to a cubic system and exhibits therefore strong correlations (see Sr_2NaIO_6 Figure 1). The model with reasonable I–O and Na–I distances together with the best GOF parameter was retained. It can be seen that the deviation from cubic symmetry increases with decreasing ion radius of the alkaline-earth metal cation. Details of the refinement as well as atomic positions can be seen in Table 1.

Figure 2 shows the structural changes, when the bigger ion Ba^{2+} is replaced by a smaller one (Sr^{2+} or Ca^{2+}). Arrows in the drawing show the displacement from the ideal position to the real structure. The tendency of the distortion can be seen as the effect is smaller for Sr^{2+} as for Ca^{2+}. It was observed

* Univ.-Prof. Dr. F. Kubel
Fax: +43-1-58801-17199
E-Mail: Frank.Kubel@tuwien.ac.at
[a] Institute of Chemical Technologies and Analytics
Vienna University of Technology
Getreidemarkt 9/164-SC
A-1060 Vienna, Austria
[b] Department of Physical Chemistry,
University of Geneva
30, quai E. Ansermet
1211 Geneva 4, Switzerland

Zeitschrift für anorganische und allgemeine Chemie ZAAC Journal of Inorganic and General Chemistry

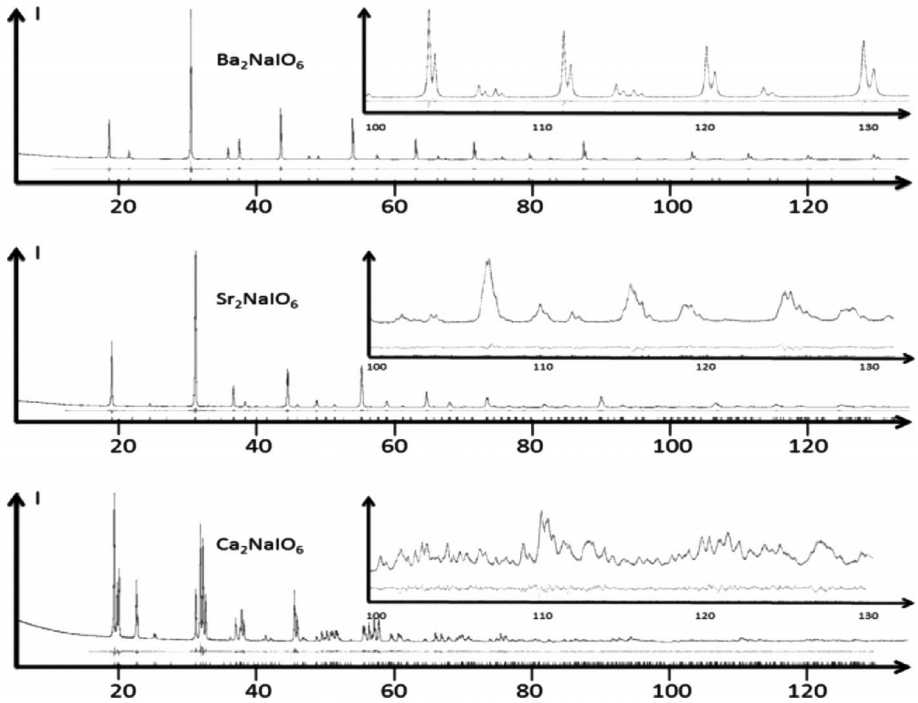

Figure 1. Observed, calculated and difference Cu-$K_{\alpha 1,2}$ – XRD pattern for M_2NaIO_6 (M = Ba, Sr, Ca) determined by Rietveld refinement using the TOPAS program.[12] Intensities between 100 and 130° are increased by a factor of 20.

Table 1. Experimental details of the crystal structure determination of the M_2NaIO_6 series with M = Ca, Sr, Ba, e.s.d.′s of the last digits in parenthesis.

Formula	Ba_2NaIO_6	Sr_2NaIO_6	Ca_2NaIO_6
Formula /g·mol^{-1}	520.55	421.13	326.05
Space group	*Fm3m* (no. 225)	$P2_1/c$ (no. 14)	$P2_1/c$ (no. 14)
Temperature /K	293	293	293
a /Å	8.3384(1)	5.7600(1)	5.5376(1)
b /Å		5.7759(1)	5.7911(1)
c /Å		9.9742(1)	9.6055(1)
β /°		125.362(1)	124.300(1)
Unit cell volume /Å^3	579.8(1)	270.61(1)	254.47(1)
Cell formula units Z	4	2	2
Density /g·cm^{-3}	5.964	5.166	4.255
Radiation wavelength /Å	1.5418	1.5418	1.5418
μ(Cu-K_α) /mm	147.42	71.4	67.8
Crystallite size /nm	439(2)	1167(2)	565(2)
2 theta min /°	15	15	15
2 theta max /°	130	130	130
2 Increment in theta /°	0.02	0.02	0.02
Number of data points	6483	6483	6483
Number of reflections	41	466	438
hkl	0.10; 0.10; 1.10	0.6; –6.6; –11.9	0.6; –6.6; –11.9
Number of variables	23	33	36
R_F /%	4.4	2.6	4.5
R_w /%	5.9	3.6	5.8
$R_{w\ expected}$ /%	1.8	1.3	1.3
R_{Bragg} /%	1.9	1.6	1.8
Goodness of fit	3.2	2.8	2.9
ICSD No.	425446	425447	425448

that interatomic distances and angles within the octahedra do not change significantly, but the octahedral-to-octahedra angle shifts (Na–O–Na) from 180° to 165.1° (Sr compound) to 140.6° (Ca compound). The octahedra are also twisted against one another. The reason therefore is the influence of the matrix effect, which is defined by the shortest alkaline earth to oxygen distance. A linear decrease was found for these distances as a function to the ionic radii. It was found that a stronger modification by putting a smaller ion as Mg^{2+} in the system did not form the desired compound. Atomic positions and interatomic

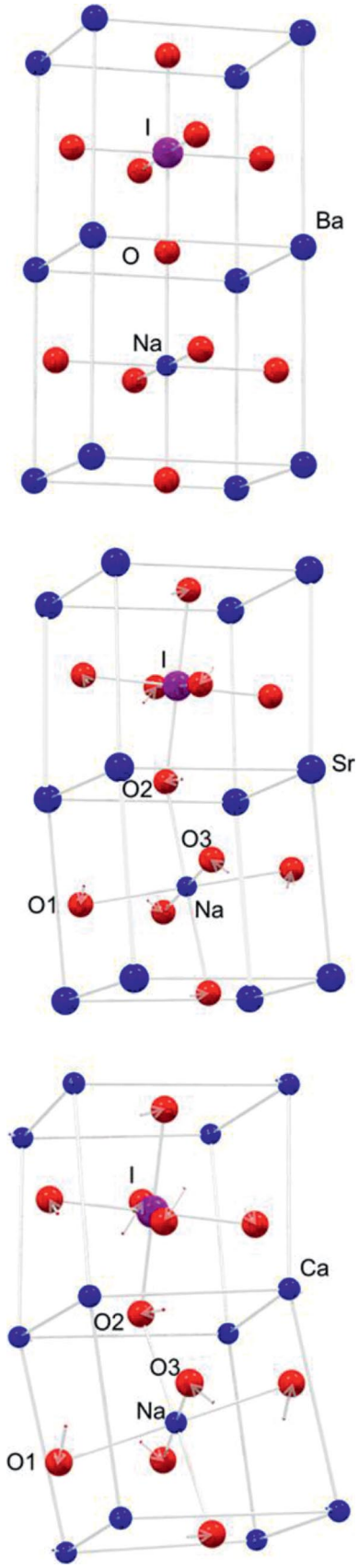

Figure 2. Deviation and shift from the idealized (cubic) to the monoclinic positions within the M_2NaIO_6 series (M = Ca, Sr, Ba). I = pink, Ba, Sr, Ca, Na = blue, O = red.

distances are given in Table 2 and Table 3 respectively. The surrounding around the alkaline-earth metal cation changes dramatically as can be seen in Figure 3.

Vibrational Spectroscopy

The symmetry analysis of the vibrations of Ba_2NaIO_6 (space group *Fm3m*) and Sr_2NaIO_6 (space group $P2_1/c$) yields the following results [the T_{1u} modes are IR active, the A_{1g}, the E_g and T_{2g} modes are Raman active in cubic symmetry, the A_u and B_u are IR active and A_g and B_g are Raman active in monoclinic symmetry (Table 4)].

In the monoclinic structure, the site group splits all degenerate mode, the crystal field further splits each line into two components.

Figure 4 compares the Raman spectra of the M_2NaIO_6 series (M = Ba, Sr, Ca). In the case of the barium compound, four bands are observed. The three bands at higher Raman shifts are assigned to the internal Raman-active bands of $[IO_6]^{5-}$ octahedra, and the band at 110 cm^{-1} to the single triply degenerate Raman-active lattice mode (T_{2g} symmetry, see Table 4). This mode corresponds to motions of the Ba^{2+} ions and it is similar to the Raman-active mode observed at 108 cm^{-1} in the cubic compound Ba_2YSbO_6.[13]

In the case of the strontium compound, a similar spectrum is observed with frequencies shifted to higher values, as would be expected by a chemical pressure effect (Sr^{2+} is smaller than Ba^{2+}). The lowest frequency bands (at 125–153 cm^{-1} and 439–454 cm^{-1}) corresponding to the two triply degenerate modes for Ba_2NaIO_6 confirm that for the strontium compound symmetry is indeed lower and leads to a splitting of these bands. A similar behavior is also observed in the Raman spectrum of the monoclinic compound Sr_2YSbO_6[13], which presents a splitting of the 414 cm^{-1} band. For the calcium compound, these splittings become even more pronounced, in agreement with its stronger distortion from cubic crystal symmetry. In this case the crystal field splitting becomes also important, leading to the observation of more than three Raman-active bonds, a total of six are predicted, for the T_{2g} modes in cubic structures.

An ab initio calculation of the isolated $[IO_6]^{5-}$ anion yielded a bond length of 2.024 Å between iodine and oxygen. Constraining this value to more realistic 1.92 Å – initially refined from a mixture of phases from our first synthesis experiments and therefore taken for the calculations – yields increased vibrational frequencies in good agreement with the experimental data for Ba_2NaIO_6. These data are collected in Table 5 and also compared with the vibrational spectra reported by *Siebert* and *Wieghard* for this compound.[14]

The calculated Mulliken charges for iodine and oxygen were found to be +2.63 and –1.27 for the unconstrained and +2.98 and –1.33 for the constrained structure, respectively, indicating a significant covalence of the iodine–oxygen bonds.

The periodic DFT calculation for Ba_2NaIO_6 revealed that the cubic structure is indeed stable, since no imaginary vibrational frequencies were found. The unit cell parameter is slightly above the experimental one [a = 8.5006 Å vs. 8.399 Å (exp)], which is often observed in the GGA approximation.[15]

Zeitschrift für anorganische und allgemeine Chemie ZAAC Journal of Inorganic and General Chemistry

Table 2. Final atomiccoordinates and equivalent isotropic displacement parameters (× 100) for the M_2NaIO_6 series (M = Ba, Sr, Ca).

Atom	x	y	z	U_{eq} [a)] /Å^2
Ba compound				
Ba	0.25	0.25	0.25	0.621(12)
I	0	0	0	0.358(14)
Na	0.5	0.5	0.5	0.53(8)
O	0.2326(3)	0	0	1.01(6)
Sr compound				
Na	0.5	0	0.5	0.40(11)
I	0	0	0	0.310(18)
Sr	0.2549(4)	0.47043(13)	0.2513(4)	0.84(2)
O1	0.240(3)	0.7330(17)	0.0401(17)	1.15(11)[c]
O2	0.1678(22)	0.0107(8)	0.2340(9)	1.15(11)[c]
O3	0.300(3)	0.1906(18)	0.0292(18)	1.15(11)[c]
Ca compound				
Na	0.5	0	0.5	0.55(8)
I	0	0	0	0.312(18)
Ca	0.2712(3)	0.44321(19)	0.25468(19)	0.72(4)
O1	0.2434(9)	0.7229(7)	0.0734(5)	1.30(8)[c]
O2	0.1127(8)	0.0562(7)	0.2252(5)	1.30(8)[c]
O3	0.3277(10)	0.1827(7)	0.0453(6)	1.30(8)[c]

a) U_{eq} = 1/3 of the trace of the orthogonalized U tensor; $U = B/8\pi^2$, c = constraint.

Table 3. Bond lengths for the M_2NaIO_6 series with M = Ca, Sr, Ba, (in Å with e.s.d.′s of last digits in parentheses).

Ba_2NaIO_6		Sr_2NaIO_6		Ca_2NaIO_6	
Na–O	2.230(3)	Na–O1	2.214(17)	Na–O3	2.224(5)
CN = 6		Na–O3	2.236(15)	Na–O2	2.301(3)
		Na–O2	2.197(6)	Na–O1	2.305(6)
I–O	1.940(3)	I–O1	1.953(13)	I–O2	1.911(5)
CN = 6		I–O2	1.943(8)	I–O3	1.927(5)
		I–O3	1.922(16)	I–O1	1.954(4)
Ba–I	3.6106(1)	I–Sr	3.4001(18)	I–Ca	3.269(1)
CN=4		I–Sr	3.5042(21)	I–Ca	3.351(1)
		I–Sr	3.543(4)	I–Ca	3.4503(22)
		I–Sr	3.6788(17)	I–Ca	3.8024(14)
Ba–O	2.9516(1)	Sr–O1	2.557(17)	Ca–O1	2.319(5)
CN = 12		Sr–O2	2.533(14)	Ca–O2	2.334(6)
		Sr–O2	2.689(5)	Ca–O2	2.365(4)
		Sr–O3	2.548(11)	Ca–O3	2.396(4)
		Sr–O1	2.768(11)	Ca–O1	2.565(4)
		Sr–O3	2.791(19)	Ca–O3	2.670(6)
		Sr–O3	2.871(18)	Ca–O3	2.727(6)
		Sr–O1	3.394(18)	Ca–O1	2.976(4)
		Sr–O2	3.150(5)	Ca–O2	3.371(5)
		Sr–O2	3.251(14)	Ca–O2	3.629(4)
		Sr–O3	3.394(11)	Ca–O3	3.637(4)
		Sr–O1	3.394(18)	Ca–O1	3.697(6)

The vibrational frequencies obtained are somewhat lower to the experimental ones (see Table 5), however, constraining the unit cell to the size of the experimental one leads to frequencies, which are very close to the experimental ones.

Conclusions

The observed transition from the cubic symmetry of Ba_2NaIO_6 to the monoclinic symmetry of Sr_2NaIO_6 is analogous to the behavior for the antimony compounds Ba_2YSbO_6 (cubic) and Sr_2YSbO_6 (monoclinic)[13]. Raman spectroscopy proves to be very useful to establish the presence of lower symmetry, which is not always obvious from powder X-ray data alone, as demonstrated in the case of Sr_2NaIO_6.

Calculations show that the discrete $[IO_6]^{5-}$ octahedron can really be regarded as an individual unit in the structure and that the bonds between the different atoms (I and O) have a strong covalent nature.

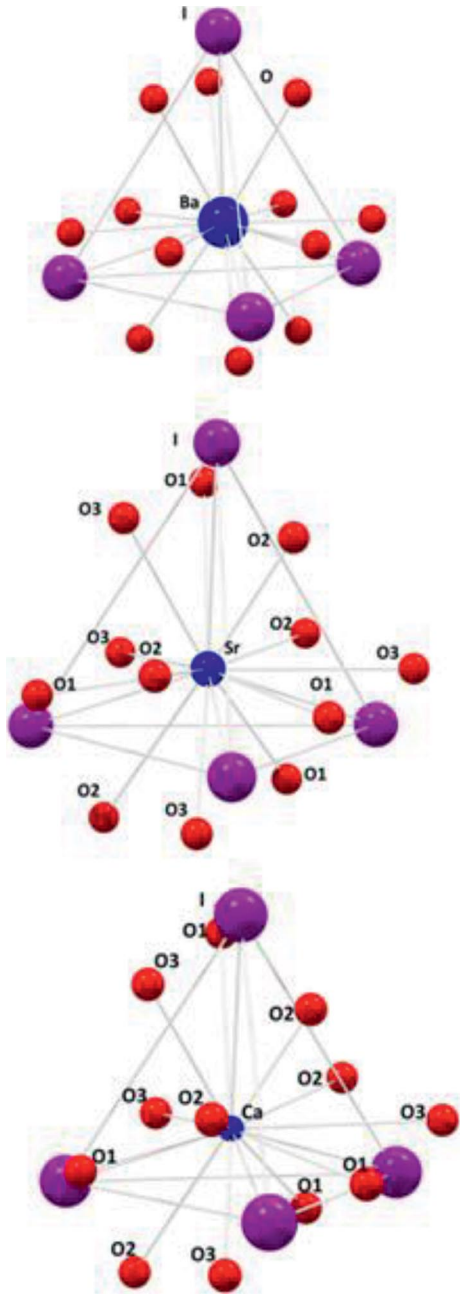

Figure 3. Oxygen environment around M = Ba, Sr, Ca in M_2NaIO_6 series (CN = 12) I = pink, Ba, Sr, Ca = blue, O = red.

Table 4. Symmetry analysis of the vibrations in the cubic and monoclinic crystal phases of the M_2NaIO_6 series (M = Ca, Sr, Ba).

	*Fm*3*m*	$P2_1/c$
Internal modes of $[IO_6]^{5-}$	$A_{1g} + E_g + 2T_{1u} + T_{2u} + T_{2g}$	$(A_g+B_g) + 2(A_g+B_g) + 6(A_u+B_u) + 3(A_u+B_u) + 3(A_g+B_g)$
Libration	T_{1g}	$3(A_g+B_g)$
Optical lattice modes	$2T_{1u} + T_{2g}$	$6(A_u+B_u) + 3(A_g+B_g)$
Acoustic modes	T_{1u}	$3(A_u+B_u)$

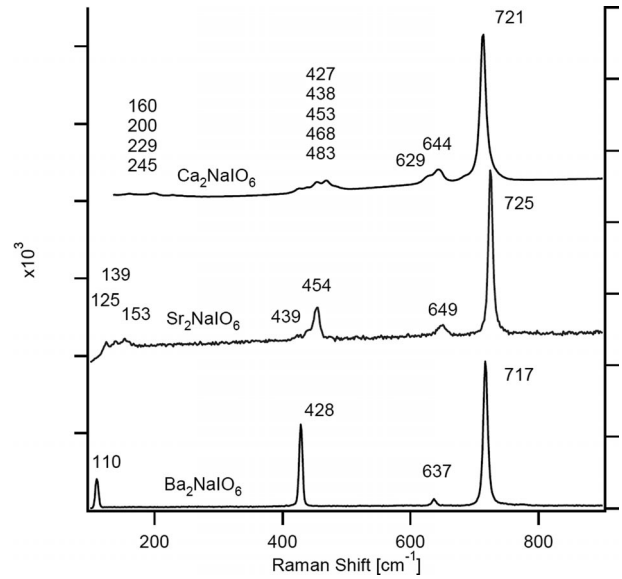

Figure 4. Raman spectra of the M_2NaIO_6 series with M = Ca, Sr, Ba (CN = 12).

Table 5. Comparison of the experimental and theoretical vibrational frequencies /cm^{-1} for $[IO_6]^{5-}$ in Ba_2NaIO_6. Abinit relaxed refers to calculation with the relaxed unit cell (a = 8.5006 Å), and abinit constrained refers to a unit cell with the experimental a parameter (a = 8.34 Å).

	A_{1g}	E_g	T_{1u}	T_{1u}	T_{2g}	T_{2u}
Abinit. relaxed	655	563	604	424	408	286
Abinit. constr.	718	624	674	450	424	307
DFT 2.024 Å	423.7	384.1	443.1	351.3	380.4	221.9
DFT 1.92 Å	669.6	609.6	669.8	436.6	411.5	220.9
Ba_2NaIO_6	717	637	673		428	
Siebert[15]	718(vs)	636(vw)	687(vs)	430(vs)	428(s)	
Sr_2NaIO_6	725	649			454 439	
					483 468	
Ca_2NaIO_6	721	644			453 438	
					427	
		622				

Experimental Section

Synthesis 1: The barium compound Ba_2NaIO_6 was first prepared from carefully dried (at 100 °C for several hours) and mechanically mixed BaF_2 (Sigma Aldrich, p.a.) and NaI (Fluka, *rein*) powders, placed in a covered platinum crucible and heated in air from room temperature to 650 °C within 3 h. The sample was kept at 650 °C for 6 h and cooled to room temperature within 10 h. This procedure was repeated 3 times. An excess of BaF_2 still present was brought to reaction by adding 30 wt-% of NaI to compensate the weight loss during the first steps, followed by careful grinding to increase the reaction surface. The final step completed the reaction according to:

$$2BaF_2 + 5NaI + 2O_2 \downarrow \rightarrow Ba_2NaIO_6 + 2I_2 \uparrow + 4NaF$$

The 33 wt-% of NaF used as mineralizator was washed out with distilled water (3×) and ethanol (2×). After drying, a single phase compound was obtained. The same reaction procedure was performed for the strontium and the calcium sample. The calculated amount of ca.

Zeitschrift für anorganische und allgemeine Chemie ZAAC Journal of Inorganic and General Chemistry

2 g of white single-phase powders was obtained by this method for all three samples.

Synthesis 2: A further independent preparation of Ba_2NaIO_6 was performed at ca 650 °C by the reaction:

$$2Ba(OH)_2{\cdot}8H_2O + NaIO_4 \rightarrow Ba_2NaIO_6 + 10H_2O \uparrow$$

The preparation of Ba_2NaIO_6 from $Ba(OH)_2{\cdot}8H_2O$ is practically stoichiometric (yield > 85 %). Starting from BaF_2, the yield is less, probably caused by the evaporation of some iodine. A preparation attempt from a nitrate melt resulted in strong iodine evaporation.

The calcium and strontium compounds were prepared with synthesis pathway 1 and the strontium compound also with synthesis pathway 2.

The analyses were carried out with the products obtained by both methods and no significant difference was found.

Analyses: Calorimetric measurements were carried out with a Netzsch STA 449 C Jupiter system in DTA/TG mode with Al_2O_3 crucibles in an argon atmosphere, thermogravimetric measurements with a Netzsch TG 209 F3 Tarsus system in nitrogen atmosphere.

SEM and EDX measurements were carried out for Ba_2NaIO_6 with a FEI Quanta 200 instrument and gave a Ba:Na:I ratio of approximately 2:2:1, close enough to the expected values for Ba_2NaIO_6.

X-ray diffraction measurements of all powders were performed with a PANalytical X'Pert PRO system, recently calibrated and optimized using a NIST-LaB_6 standard (emission profile, instrument function, tube tails), with primary and secondary Soller slits of 0.04 rad, a fixed divergence slit of 0.5°, a fixed antiscatter slit of 1° and a 200 mm goniometer radius. Silicon zero background platelets for flat samples were used. Measuring time: 180 min, 5–135° in 2Θ°, Cu-K_α radiation, X'Celerator detector with Ni-K_β filter, where the scan length was ca. 2.55. The evaluation and Rietveld refinements with the fundamental parameters approach were performed with the TOPAS[12] software. Amongst others the refined parameters were 6 background points, strain, crystallite size, zero point, absorption, positional parameters and vibrational parameters.It should be mentioned that for the refinement of Ba_2NaIO_6, it is necessary to take (111) and (100) texture into account. It can be seen in Figure 5 that the crystals are relatively big and exhibit a pronounced crystal shape. Therefore the crystals orient apparently in these directions during the powder compaction for XRD measurements.

IR spectra were obtained with a Perkin-Elmer Spectrum 100 Instrument in conjunction with a Specac ATR setup. Raman spectra were measured with a 488 nm LASER and a Holospec monochromator equipped with a liquid nitrogen cooled CCD camera. Further Raman experiments were done with a Renishaw Raman microscope using 532 nm LASER excitation.

Theoretical Calculations: The optimization and frequencies calculations were performed on the isolated $[IO_6]^{5-}$ ion by using the Gaussian 09 package.[16] The B3LYP[17–19] functional, 6-31g(dp) basis set for oxygen atoms and lanl2dz basis set for the iodine atom were chosen.

The frequency calculations were performed on the $[IO_6]^{5-}$ ion completely relaxed and on the one, in which the I–O distances were kept equal to 1.92 Å.

Periodical DFT Calculations on Ba_2NaIO_6: The optimization and frequency calculations were performed by using the ABINIT package[20–22] within General Gradient Approximation (GGA).[23–24] In the optimization a kinetic energy cutoff of 70 Hartree and a Monkhorst-Pack grid[25] of $10 \times 10 \times 10$ were used. A first calculation was done for an optimized structure, a second one with the unit cell parameter constrained to the experimental value. In both cases a convergence problem at the level of application of perturbation theory was noticed.

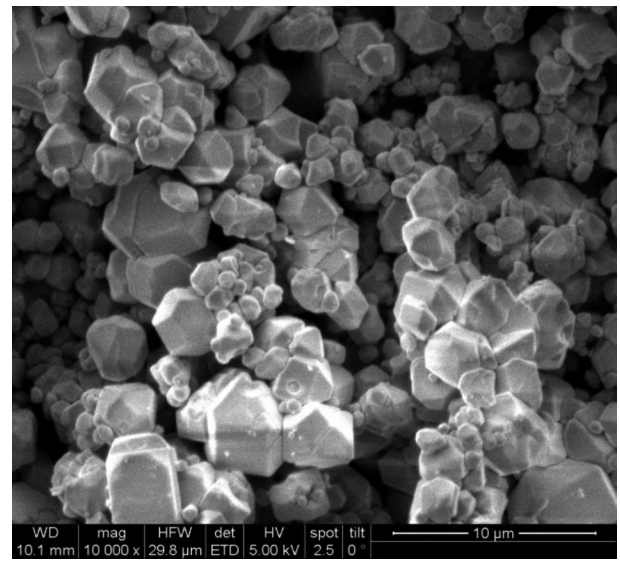

Figure 5. SEM image of Ba_2NaIO_6. Pronounced crystal faces require the use of a texture model during the refinement.

Further details of the crystal structure investigations may be obtained from the Fachinformationszentrum Karlsruhe, 76344 Eggenstein-Leopoldshafen, Germany (Fax: +49-7247-808-666; E-Mail: crysdata@fiz-karlsruhe.de, http://www.fiz-karlsruhe.de/request for deposited data.html) on quoting the depository numbers CSD-425446 (for Ba_2NaIO_6), CSD-425447 (for Sr_2NaIO_6), and CSD-425448 (for Ca_2NaIO_6).

Acknowledgements

The authors want to thank *Dr. Erich Halwax* (TU Wien) for helpful discussions, *Elisabeth Eitenberger* (TU Wien) for SEM and EDX measurements and *Mr. Cedric Schnyder* (Muséum d'Histoire Naturelle Genève) for the Raman measurements with the Renishaw instrument. The assistance of *Juan Carlos Fallas* and *Loic Musy* during the initial synthesis is gratefully acknowledged. The X-ray centre of the Vienna University of Technology is acknowledged for providing access to the powder diffractometer. This work was supported by the Swiss National Science Foundation.

References

[1] Y.-H. Huang, G. Liang, M. Croft, M. Lehtimäki, M. Karppinen, J. B. Goodenough, *Chem. Mater.* **2009**, *21*, 2319–2326.
[2] S. Baidya, T. Saha-Dasgupta, *Phys. Rev. B* **2012**, *86*, 024440.
[3] B. Moreno, E. Urones-Garrote, E. Chinarro, L. Fuentes, E. Morán, *Chem. Mater.* **2011**, *23*, 1779–1784.
[4] D. E. Bugarisa, J. P. Hodgesb, A. Huqb, H.-C. zur Loye, *J. Solid State Chem.* **2011**, *184*, 2293–2298.
[5] J. E. Greedan, S. Derakhshan, F. Ramezanipour, J. Siewenie, Th. Proffen, *J. Phys. Condens. Matter* **2011**, *23*, 164213.
[6] X. Yin, Y. Wang, F. Huang, Y. Xia, D. Wan, J. Yao, *J. Solid State Chem.* **2011**, *184*, 3324–3328.

[7] H. T. Stokes, E. H. Kisi, D. M. Hatch, C. J. Howard, *Acta Crystallogr., Sect. B* **2002**, *58*, 934–938.
[8] T. Birchall, C. S. Frampton, G. J. Schrobilgen, J. Valsdottir, *J. Phys. Chem.* **1990**, *94*, 6503–6506.
[9] A. W. Sleight, J. Longo, R. Ward, *Inorg. Chem.* **1962**, *1*, 245–250.
[10] S. Schneider, R. Hoppe, *Z. Anorg. Allg. Chem.* **1970**, *376*, 268–276.
[11] S. Naray-Szabo, K. Sasvari, *Z. Kristallogr.* **1938**, *99*, 27–31.
[12] *TOPAS*, Version 4.2, Bruker AXS GmbH, Karlsruhe, Germany, **2009**.
[13] F. Fernandez-Martinez, J. L. Montero, I. Carrillo, C. Colon, *J. Alloys Compd.* **2012**, *538*, 34–39.
[14] H. Siebert, G. Wieghardt, *Z. Naturforsch.* **1972**, *27b*, 1299–1304.
[15] V. D'Anna, L. M. Lawson Daku, H. Hagemann, *Phys. Rev. B* **2010**, *82*, 24108.
[16] *Gaussian 09*, Revision A.1, M. J. Frisch, G. W. Trucks, H. B. Schlegel, G. E. Scuseria, M. A. Robb, J. R. Cheeseman, G. Scalmani, V. Barone, B. Mennucci, G. A. Petersson, H. Nakatsuji, M. Caricato, X. Li, H. P. Hratchian, A. F. Izmaylov, J. Bloino, G. Zheng, J. L. Sonnenberg, M. Hada, M. Ehara, K. Toyota, R. Fukuda, J. Hasegawa, M. Ishida, T. Nakajima, Y. Honda, O. Kitao, H. Nakai, T. Vreven, J. A. Montgomery Jr., J. E. Peralta, F. Ogliaro, M. Bearpark, J. J. Heyd, E. Brothers, K. N. Kudin, V. N. Staroverov, R. Kobayashi, J. Normand, K. Raghavachari, A. Rendell, J. C. Burant, S. S. Iyengar, J. Tomasi, M. Cossi, N. Rega, J. M. Millam, M. Klene, J. E. Knox, J. B. Cross, V. Bakken, C. Adamo, J. Jaramillo, R. Gomperts, R. E. Stratmann, O. Yazyev, A. J. Austin, R. Cammi, C. Pomelli, J. W. Ochterski, R. L. Martin, K. Morokuma, V. G. Zakrzewski, G. A. Voth, P. Salvador, J. J. Dannenberg, S. Dapprich, A. D. Daniels, Ö. Farkas, J. B. Foresman, J. V. Ortiz, J. Cioslowski, D. J. Fox, Gaussian, Inc., Wallingford CT, USA, **2009**.
[17] A. D. Becke, *J. Chem. Phys.* **1993**, *98*, 1372–1377.
[18] A. D. Becke, *J. Chem. Phys.* **1993**, *98*, 5648–5652.
[19] *Gaussian NEWS*, Vol. 5, no. 2, Summer **1994**, p. 2., Becke3LYP Method References and General Citation Guidelines.
[20] X. Gonze, J.-M. Beuken, R. Caracas, F. Detraux, M. Fuchs, G.-M. Rignanese, L. Sindic, M. Verstraete, G. Zerah, F. Jollet, M. Torrent, A. Roy, M. Mikami, P. Ghosez, J.-Y. Raty, D. Allan, *Comput. Mater. Sci.* **2002**, *25*, 478–492.
[21] X. Gonze, G.-M. Rignanese, M. Verstraete, J.-M. Beuken, Y. Pouillon, R. Caracas, F. Jollet, M. Torrent, G. Zerah, M. Mikami, P. Ghosez, M. Veithen, J.-Y. Raty, V. Olevano, F. Bruneval, L. Reining, R. Godby, G. Onida, D. R. Hamann, D. C. Allan, *Z. Kristallogr.* **2005**, *220*, 558–562.
[22] *ABINIT Code*, a common project of the Université Catholique de Louvain, Corning Incorporated, the Université de Liège, the Commissariat á l'Energie Atomique, Mitsubishi Chemical Corp., the Ecole Polytechnique Palaiseau, and other contributors, http://www.abinit.org.
[23] J. P. Perdew, K. Burke, M. Ernzerhof, *Phys. Rev. Lett.* **1996**, *77*, 3865–3868.
[24] J. P. Perdew, K. Burke, M. Ernzerhof, *Phys. Rev. Lett.* **1997**, *78*, 1396.
[25] H. J. Monkhorst, J. D. Pack, *Phys. Rev. B* **1976**, *13*, 5188–5192.

Received: December 19, 2012
Published Online: April 18, 2013

